Design and Characterization of the Notre Dame STEM Mach 6 Ludwieg Tube

Jacob M. Caldwell *, Alec C. Jobbins †, Alyssa Spencer ‡, William D. Jordan §, Eric Matlis ¶, and Thomas C. Corke ‖
University of Notre Dame, Notre Dame, Indiana, 46556

The University of Notre Dame has designed and constructed a new Mach 6 Ludwieg tube for the purpose of hypersonics research and education. The tunnel uses a fast acting plunger valve to actuate the flow, providing run times of 55 ms. The Mach 6 flow is generated through a 0.28 meter diameter nozzle. Pitot pressures are measured on the centerline, and with a rake. The nominal Mach number was found to be 5.8 and pitot pressure fluctuations were 1.5%, both varying with unit Reynolds number. Possible air liquefaction is present at high Reynolds numbers, which is apparent from a rise in noise.

I. Nomenclature

l	=	axial position of plunger from fully opened position
M	=	Mach number
p'	=	pressure fluctuation measured by stagnation probe
P_0	=	stagnation pressure
r	=	radial distance from nozzle centerline
R	=	gas constant of air
Re'	=	unit Reynolds number
R_p	=	radius of plunger housing
t	=	time
T_0	=	stagnation temperature
x	=	axial distance from nozzle throat
R_t	=	reduced radius of the front of the plunger
m_p	=	mass of the plunger
γ	=	ratio of specific heats
θ	=	azimuthal angle in measurement plane

II. Introduction

Ludwieg tubes have become a common way to conduct hypersonic research due to their cost-effective nature. Requiring less infrastructure than blowdown style tunnels, they allow hypersonic research at a university level. As part of the Hypersonic Systems Initiative at the University of Notre Dame, a Mach 6 Ludwieg tube was designed and built to support both research and education. The goal of this paper is to outline the design of the tunnel, and report initial operating characteristics.

Many authors have detailed the operation of Ludwieg tubes in depth [1],[2]. In brief, a Ludwieg tube contains a high and low pressure side. The high pressure side contains the driver tube, while the low pressure side contains the nozzle and test section. When actuated sufficiently fast, by a valve or burst diaphragm, an expansion wave moves upstream in the driver tube, accelerating the air. As the wave travels upstream, constant stagnation conditions are maintained upstream of the nozzle until the expansion returns to the throat of the nozzle. At this point, the wave is reflected, leading

*Ph.D student, Department of Aerospace and Mechanical Engineering, and AIAA Student Member.
†Ph.D student, Department of Aerospace and Mechanical Engineering, and AIAA Student Member.
‡Ph.D student, Department of Aerospace and Mechanical Engineering, and AIAA Student Member.
§Ph.D student, Department of Aerospace and Mechanical Engineering, and AIAA Student Member.
¶Research Assistant Professor, Department of Aerospace and Mechanical Engineering, and AIAA Associate Fellow
‖Clark Chair Professor, Department of Aerospace and Mechanical Engineering, and AIAA Fellow.

to a drop in stagnation pressure. Using a long driver tube, run times can be achieved in the hundreds of millisecond range, potentially including multiple reflections.

Detailed knowledge of flow characteristics is imperative for any research conducted in a wind tunnel. The primary characteristics of interest are the Mach number throughout the nozzle and test section, freestream pressure fluctuation levels throughout the nozzle and test section, and the minimum stagnation temperature (as a function of unit Reynolds number) that experiments can be conducted at without experiencing condensation in the freestream. The present experiments document the first two of these flow characteristics in the Notre Dame STEM Mach 6 Ludwieg Tube using traditional stagnation pitot probes.

III. Facility Design

A. Overview

The Notre Dame STEM Mach 6 Ludwieg Tube was designed to fit within the Hessert Laboratory for Aerospace Research. The tunnel is comprised of a (1) driver tube, (2) plunger valve, (3) axisymmetric converging-diverging nozzle and a (4) free-jet test section. These components are labeled in Fig. 1. The operating conditions are found in Table 1. Further details of the component design are discussed in the remainder of this section.

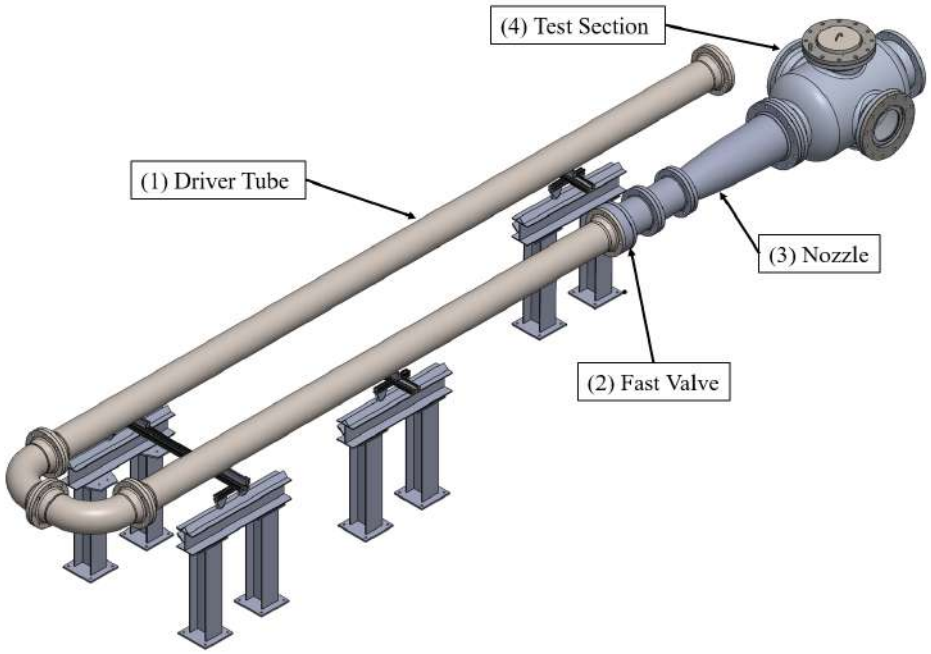

Fig. 1 CAD Rendering of ND STEM M6LT

Table 1 ND STEM M6LT Operating Conditions

Mach No.	P_0 **[kPa]**	T_0 **[K]**	**Re'** [10^6/m]	**Run Time [ms]**
5.8	620-1720	310-480	5.6-17	60

B. Driver Tube

The driver tube of Ludwieg tunnels defines the run time and conditions of the test. The longer it takes for the expansion wave to return to the throat, the longer constant conditions are maintained in the flow[2]. Thus, the ND

STEM M6LT driver tube was designed to maximize run time, while fitting within the lab space. To do this, the driver tube uses a "U" shape to increase the length while staying within the confines of the room. Tunnels, such as the AFRL Ludwieg tube [3], have used this design before with no effect on the quality of the run. To achieve the bend, two 90° bends were used. With these constraints, the length of the driver tube was designed to be 12 meters.

The driver tube also supplies the stagnation conditions to the tunnel. To contain the pressure, size 8 schedule 40 304 stainless steel pipes were selected as they were readily available and were capable of maintaining the desired stagnation pressure of 1700 kPa (250 psia). The pressure is supplied by two Sauer 2711 compressors. In addition to pressure, the stagnation temperature must be elevated to avoid nitrogen liquefaction within the test section [4]. Heating the driver tube air is done through the use of resistive heaters, mounted to the exterior of the pipe. These heaters are capable of exceeding the liquefaction temperature of any expected operating conditions.

Due to the short run times of Ludwieg tubes, and the use of a fast valve, not all the air is expelled during the run. Some cost can be saved by only heating a portion of the air to the desired temperature. However, heating only a portion cannot be done without any alterations to the driver tube. If there exists a temperature gradient along the driver tube within the air, premature wave reflections can occur, causing the steady flow time to be cut short. As outlined by Estorf et al. [1], Eq. 1 is a simple modification to the diameter of the pipe in the heated region. The hot region, denoted by "h", has a reduced diameter from the cold, "c", region.

$$A_c \cdot \sqrt{T_c} = A_h \cdot \sqrt{T_h} \tag{1}$$

The length of the heated section can then be computed by finding the mass of air that is expelled during the time of the run. The time of the a run is only a function of the speed of sound and length of the driver tube. With these values, the run time is estimated at 60 ms. In that amount of time, 0.18 kg of air is expelled through the nozzle at maximum operating conditions, which equates to a region of 180 mm in diameter and 500 mm long. In the final design, a length of 1 m was used to ensure plenty of air was available in case multiple reflections were used.

C. Fast Acting Plunger Valve

The actuation method for the ND STEM M6LT is a fast acting plunger valve designed in-house for this tunnel. It uses the same concept as other plunger valves [1], [3], using the air of the driver tube to open/close the valve. The benefits of fast acting valves, over the alternative of burst diaphragms, include fast reload times and low operational cost. The valve operates using the pressure difference between the driver tube and the cavity behind the valve. When the pressures are equal, the valve is closed. To open, the pressure behind the valve is released to atmosphere, forcing the valve open.

The process of opening the valve needed to be modeled such that the opening time could be predicted and optimized. Using a control volume around the cavity behind the valve, Eq. 2 can be written. The rate change in pressure, p, can be described by taking the derivative with respect to time of the ideal gas equation.

$$\frac{dp}{dt} = \frac{\dot{m}RT - p\pi R_p^2 \frac{dl}{dt}}{\pi R_p^2 l} \tag{2}$$

Where the mass flow rate can be defined, under the assumption of choked flow, by Eq.3

$$\dot{m} = A_v p \sqrt{\frac{\gamma}{RT}\left(\frac{2}{\gamma+1}\right)^{\frac{\gamma+1}{\gamma-1}}} \tag{3}$$

Where A_v is the minimum area in the air line that vents the cavity of the valve. Plugging Eq. 3 into Eq. 2, and making the assumption that $\frac{dp}{dt} \approx \frac{\Delta p}{\Delta t}$ for small Δt, p_{i+1} in Eq. 4 can be computed by stepping through t, where i denotes the current step in time.

$$p_{i+1} = p_i \left(\frac{\sqrt{\gamma RT\left(\frac{2}{\gamma+1}\right)^{\frac{\gamma+1}{\gamma-1}}} A_v - \pi R_p^2 \left(\frac{dl}{dt}\right)_i}{\pi R_p^2 l_i} \Delta t + 1 \right) \tag{4}$$

The motion of the valve, dl/dt & l, can be found using the equations of motion, where the acceleration is found

using Eq. 5, which is a force balance on the plunger.

$$a_{i+1} = \frac{p_{i+1}\pi R_p^2 - P_0\pi(R_p^2 - R_t^2)}{m_p} \tag{5}$$

Where m_p is the mass of the plunger and R_t is the reduced radius of the front of the plunger. The plunger, however, does not start moving until $P_0 R_t^2 > p_i R_p^2$, so the acceleration is not computed until this requirement is met. With initial conditions of $p_1 = P_0$, $dl/dt = 0$, and l is the total travel of the valve, the motion can be predicted. First, p_{i+1} is computed using Eq. 4, followed by computing the new acceleration of the valve with Eq. 5. The acceleration is then used to compute the speed and new position of the valve with the equations of motion. The process is then repeated until l reaches 0. Using this method, values of A_v, R_t, R_p and l were simulated to give a fast opening time, fit within the driver tube and provide enough sealing surface against the nozzle. Fig. 2 shows the predicted motion of the final version of the valve, with a predicted opening time of approximately 20 ms.

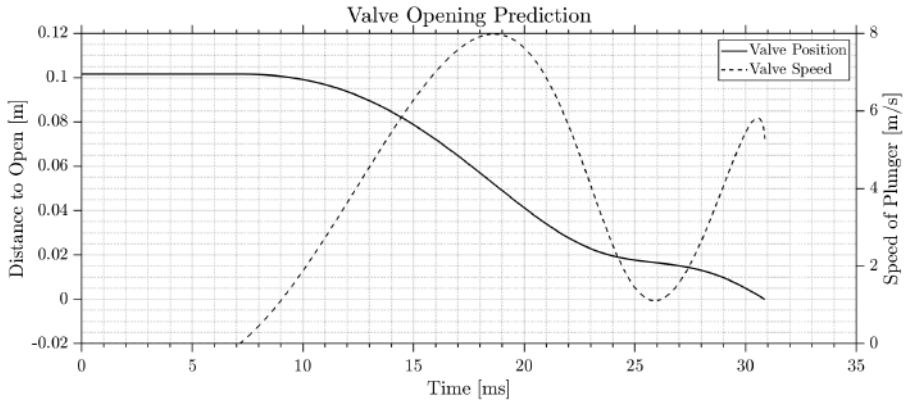

Fig. 2 Predicted Valve Opening

An exploded view of the final valve design is in Fig. 3. The valve was built into two pieces, the plunger and the housing. The housing mounts as one piece, in between the driver tube and nozzle, allowing it to be completely removed for maintenance. The plunger was a combination of a base and a tip. The tip is made from both PTFE and aluminum. The PTFE provides the seal between driver tube and nozzle and was used reduce any damage to the nozzle upon repeated closing motions. The PTFE was held in place by the aluminum tip brought together using a bolt through its center.

The base of the plunger was a hollow piece of 6061-T6 to reduce the weight. This increases acceleration, and reduces the impact on opening and closing. The base also included grooves on the exterior which housed bronze filled PTFE wear rings which provided a dynamic seal and low friction between the plunger and housing. Finally, the bottom of the plunger included a groove that fit a -419 O-ring to dampen the opening impact on the housing.

Operating the plunger valve is done using two solenoid valves integrated into an existing PLC system. One solenoid feeds the high pressure air to the cavity behind the plunger. This operation closes the valve. The other solenoid operated to exhaust the cavity behind the plunger, which opens the valve. The same process is used by the Ludwieg tube located at Air Force Academy [5].

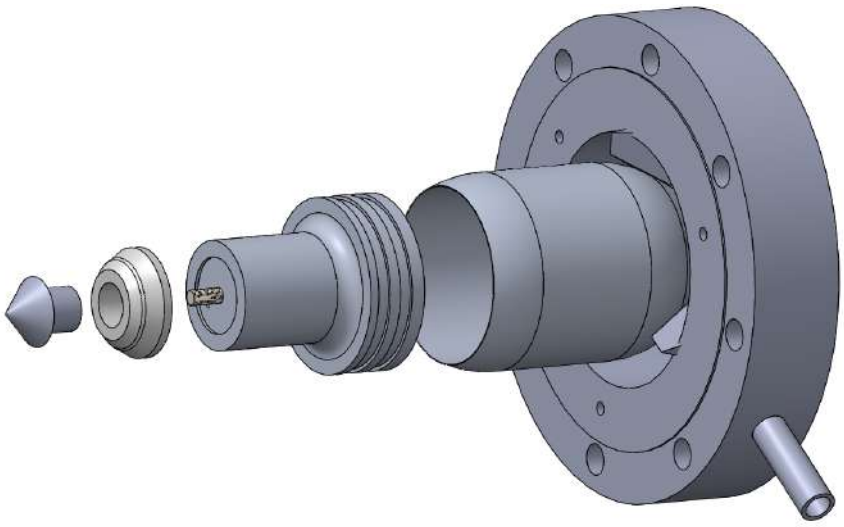

Fig. 3 CAD of Final Valve Design

D. Nozzle

To produce the hypersonic flow within the test section, an axisymmetric converging-diverging nozzle was designed. Similar to the driver tube, length needed to be limited to fit within the room. The contour for the expanding part of the nozzle was created using a method of characteristics code developed by Sivells [6]. The contour was generated without viscous corrections, as any variations in the final Mach number were not a concern. The expansion was finalized with an exit diameter of .28 m, and 1.5 m in length. The contour for the converging section of the nozzle was created using a match cubic, matching the throat of the expansion to the diameter of the driver tube. The final nozzle is seen in Fig. 1, and was designed to minimize the number of flange connections. Four total sections were used, due to restrictions from the manufacturer.

E. Test Section

The ND STEM M6LT is a free jet facility, where the nozzle exits into a 0.6 m diameter section. The test section is held near vacuum by an Edwards nEs220 Single Stage vacuum pump that can bring the pressure down to 0.1 mbar, and is connected to a larger dump tank that is shared by several facilities. The test section features three windows, 0.3 m in diameter, two on the sides and one on top. Inside the test section, a T-slotted plate is fixed to the bottom for model mounting, and is 1.1m in length. The test section can be seen in Fig.1.

IV. Experimental Setup

A. Stagnation Pitot Probe Design & Measurements

To evaluate noise levels in the ND STEM M6LT, a Stagnation Pitot Probe (SPP) was instrumented (flush mounted) with an XCE-062-1.7BARA (B Screen) Kulite, which has a mechanical natural frequency of 240 kHz. An upper limit on the sensor's usable frequency range is imposed by a cavity resonance introduced by the B Screen. This cavity resonance was observed to occur just above 50 kHz in this experiment, which is consistent with observations by Munoz et al. [7]. The root mean square fluctuation values were computed via integrating the power spectral density (PSD) of the mean-removed, calibrated signal from 0-50 kHz and then taking the square root. Noise levels were then computed by normalizing this result by the mean pressure measurement. This method was presented by Steen [8], Sweeney [9], and others in the documention of noise levels for the Boeing/AFOSR Mach-6 Quiet Tunnel in order to prevent the contribution of the aforementioned nonphysical resonances, and has since become a standard method of computing noise levels for Kulite measurements. As seen in Fig. 4, cutting off the integration at 50kHz captures most of the physical noise while avoiding the B Screen resonance contribution, and noise contributions at frequencies higher than the B Screen resonance are comparatively small.

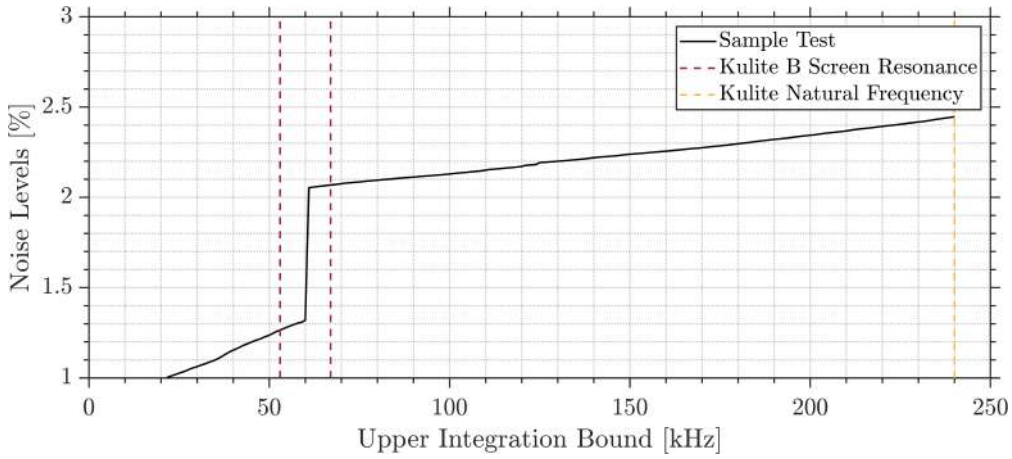

Fig. 4 Computed noise vs. upper frequency bound used in integration

The design of the SPP was based on the design used by Munoz et al. [7] in order to stay consistent with noise level measurements of other conventional Mach 6 Ludwieg Tubes. In particular, this probe features an 8 mm outer diameter with a 2 mm tip radius. Direct numerical simulations (DNS) by Ali et al. [10] showed that the rounded tip remedied an overestimation of pressure fluctuations seen with flat-faced cylindrical probes due to a constructive interference via the reflection of acoustic disturbances between the probe's front surface and the shock wave in front of the probe. In addition, chamfered probes may introduce unwanted artifacts in the measurement's PSD due to a local flow separation [10]. The SPP and its support, installed in the ND STEM M6LT, is shown in Fig. 5.

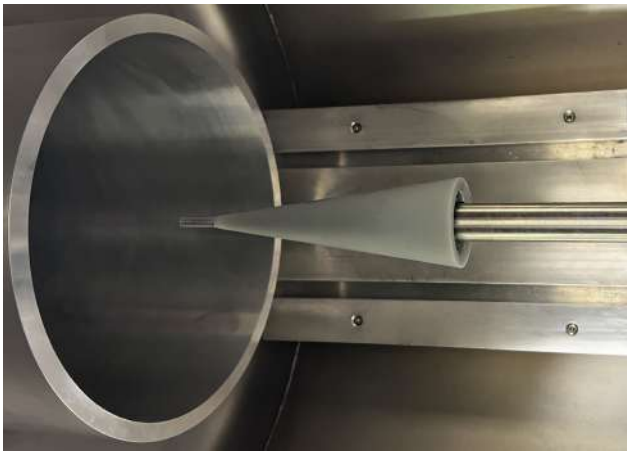

Fig. 5 SPP Support Top Down View

B. Pitot Rake Measurements

To further characterize the Mach number and noise levels of the tunnel, a traversing pitot rake was designed and built. This pitot rake was designed to be inexpensive and motorized to utilize the short downtime between runs of the tunnel with the fast valve. A linear traverse with a traverse length of 400 mm was used to move the pitot rake in the axial direction of the nozzle. To save cost and time, many parts were 3D printed in PLA with high infill percentages on an Ender 3 Pro and a Bambu Labs X1E. The rake head can accommodate up to eight sensors. One sensor is placed on the centerline, the next sensor is spaced 1 in. (25.4 mm) from the center line, and the remaining sensors are spaced 5/8 in. (15.88 mm) from each other. The sensor closest to the nozzle wall was designed to be 1/4 in. (6.35 mm) from the nozzle wall at the exit plane. The steel tube that houses the flush-mounted sensor is movable so that each radial position does not require a sensor, and a low number of total sensors can be used to capture each radial location. The

rake head is rotated by a stepper motor using a worm gear mechanism with an 80:1 gear ratio. Stepper motors and a microcontroller are used to control the axial and angular position of the pitot rake. Two Kulite XCE-062-1.7BARA (B Screen) pressure transducers were used to measure the mean and fluctuating total pressure. Figure 6 shows the pitot rake in the test section of the ND STEM M6LT .

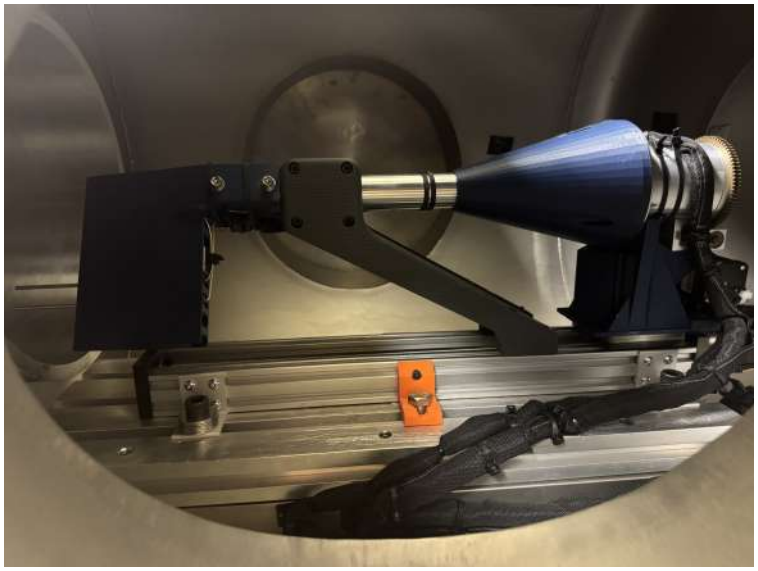

Fig. 6 Pitot rake mounted in the ND STEM M6LT

V. Results

To understand the Mach number and noise level variation throughout the ND STEM M6LT, measurements were taken at varying axial and radial locations in the nozzle. In addition, noise levels were documented at the nozzle exit plane between unit Reynolds numbers of 6×10^6 m^{-1} and 17×10^6 m^{-1}. A summary of unique test cases is given in Table 2.

Table 2 Summary of Test Cases

Purpose of Study	T_0 **[K]**	P_0 **[kPa]**	x **[m]**	r **[mm]**	**Instrumentation**
Mach & Noise vs. Reynolds Number	{431, 446, 462, 477.5}	620 → 1654	1.48	0	Single Point SPP
Mach & Noise Contours	477.5	1152	{1.15,1.30, 1.45}	{0, 25, 41, 57, 73, 89}	Rake

Stagnation pressures and temperatures were calculated from the measured storage conditions in the driver tube via the method described by Cable et al. [2]. The storage pressure was directly measured, while the storage temperature was assumed to be in equilibrium with the driver tube wall temperature. Each test was spaced out by a minimum of eight minutes to improve the validity of this assumption as much as possible.

A. Mach Number Characterization

To calculate the Mach number of the flow, Eq. 6 was used, which is derived from isentropic and normal shock relations for a perfect gas. The Rayleigh pitot tube equation was not utilized in this case, since there is not a static port to measure the static pressure of the free stream. Equation 6 relates the total pressure of the driver tube, p_{01}, to the total pressure that is measured by the sensor behind the normal shock, p_{02}, to determine the Mach number of the flow.

$$\frac{p_{02}}{p_{01}} = \left[\frac{(\gamma+1)^2 M^2}{4\gamma M^2 - 2(\gamma-1)}\right]^{\frac{\gamma}{\gamma-1}} \left[\frac{1-\gamma+2\gamma M^2}{\gamma+1}\right] \left[1+\frac{\gamma-1}{2}M^2\right]^{\frac{-\gamma}{\gamma-1}} \tag{6}$$

A bisection method was then used to solve Eq. 6 to determine the Mach number of the flow.

To investigate the Mach number at the nozzle exit as a function of freestream unit Reynolds number, five tests were run for each Re' with the SPP, and the results were averaged. Fig. 7 displays the measured Mach number across varying freestream unit Reynolds numbers for four unique stagnation temperatures, including ± 1 standard deviation of random uncertainty. For the two lower temperatures, the upward trend in Mach number with respect to unit Reynolds number is broken for high Reynolds numbers, indicating possible condensation in the test section at these conditions since it is expected that Mach number slightly increases with increasing Re' for a viscous nozzle with an isentropic core flow. For most conditions that the Notre Dame STEM Mach 6 Ludwieg Tube will be operating in, the Mach number can be reported as 5.83 ± 0.05.

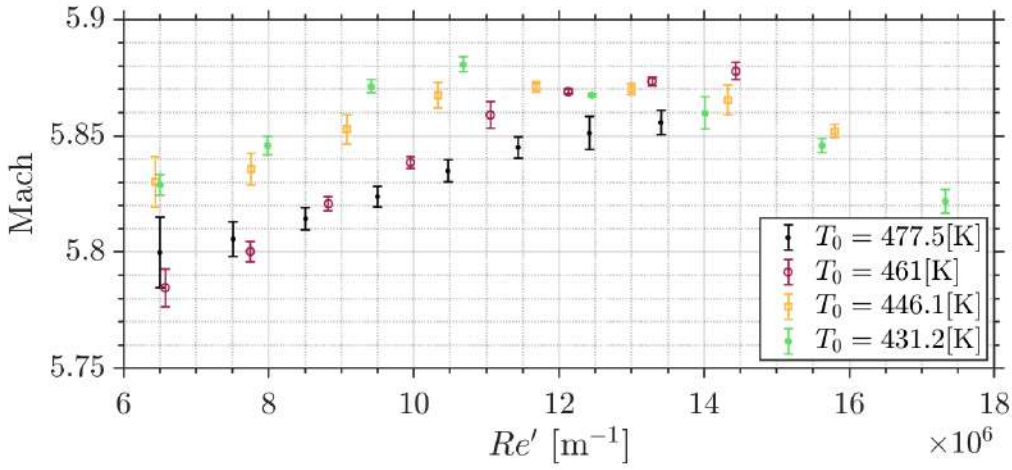

Fig. 7 Mach number vs. freestream unit Reynolds number across four unique stagnation temperatures

For comparison to the experiment, a steady-state axisymmetric CFD simulation was run in Ansys Fluent. The geometric domain was the 1.95 meter converging-diverging nozzle, including the fast-acting plunger valve in the open position. The simulation used the $k-\omega$ SST turbulence model and Sutherland's law for viscosity. The global maximum mesh element size was 0.5 mm. Mesh refinements were made in regions of high gradients such as near the throat and valve. A 30-layer inflation layer was used to refine the boundary layer on both the nozzle and valve with a wall-normal growth rate of 1.2. The maximum wall y^+ value was recorded as 0.51, which occurred on the valve surface. The maximum wall y^+ on the nozzle surface was 0.23 at the nozzle throat. The total number of elements was $1,622,194$. The inlet boundary was set to a stagnation temperature of $T_0 = 477.5$K and a stagnation pressure of $P_0 = 1152$kPa, corresponding to a freestream $Re' \approx 10.3 \times 10^6$ m^{-1}, which are the same conditions that the rake experiments were run at. Mach contours of the nozzle are displayed in Fig. 8, which indicates a Mach number of approximately 5.79 at the outlet. The nozzle simulation shows good agreement with the experimental results.

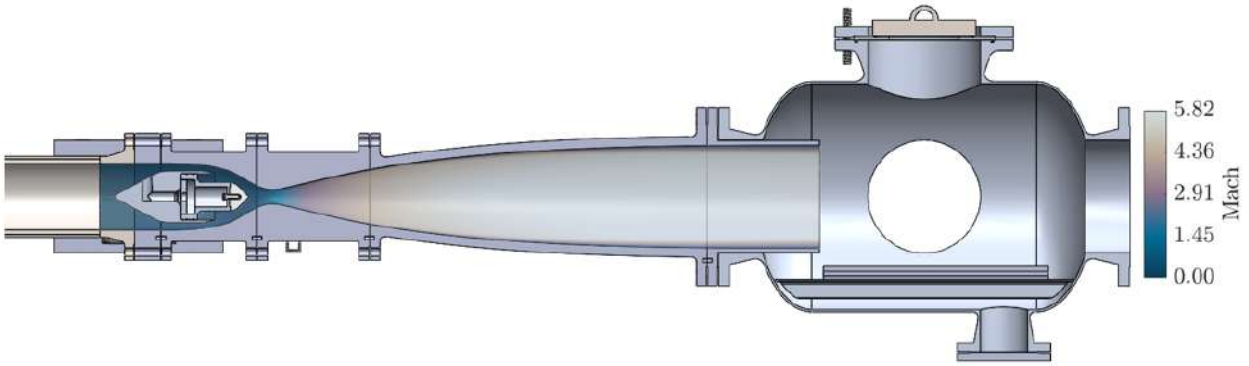

(a) Global range of Mach numbers in nozzle

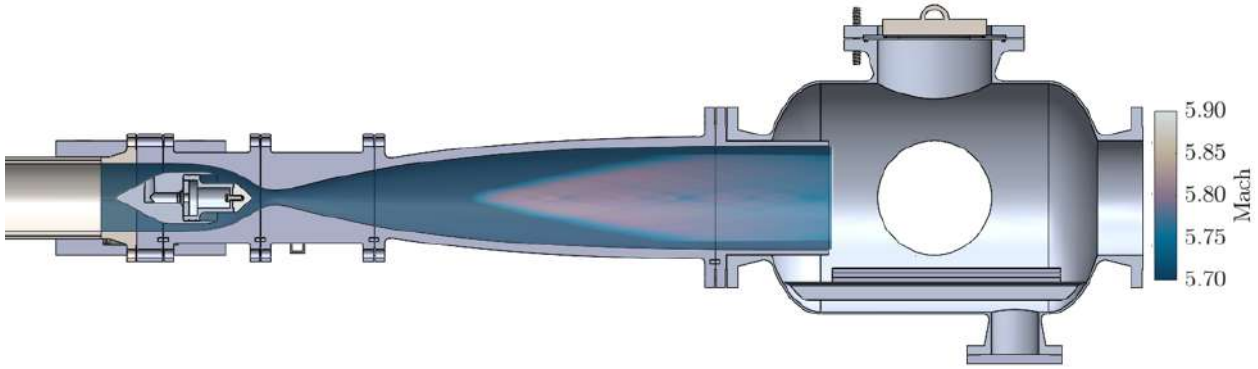

(b) Mach number ranging from 5.7 to 5.9 to illustrate shape of core flow

Fig. 8 Mach contours from axisymmetric, steady state RANS simulation which included the nozzle and the plunger valve in the open position

The motorized pitot rake measurements of total pressure, used to calculate Mach number and noise levels, were taken at three axial locations and five radial locations as shown in Table 2. The maximum radial position was not measured for the x=1.30, 1.15 m planes due to the sensors no longer working past this point during testing. Figure 9 shows the Mach number contour at x = 1.45 m. In this contour the radial position is incomplete due to sensor failure. Overall this contour shows that the Mach number is uniform, with the variation across the entire contour being minimal. The average Mach number across the entire contour is M = 5.80.

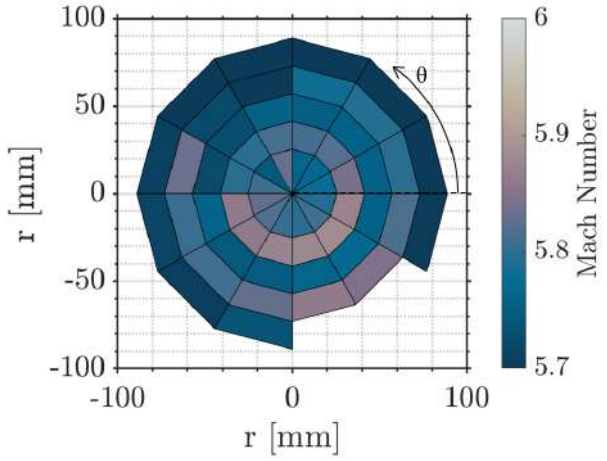

Fig. 9 Mach number contour at x = 1.45 m

Similarly, Figs. 10 & 11 show the Mach number contours at the additional axial locations, and in these contours, it is also seen that the overall variation in the Mach number is also very minimal. The average Mach numbers across these contours are 5.80 and 5.82, respectively. Overall, these Mach contour results show that in the planes of interest, the Mach number is consistent and uniform. This is of interest for putting longer models in the tunnel, as some must be relatively far into the nozzle.

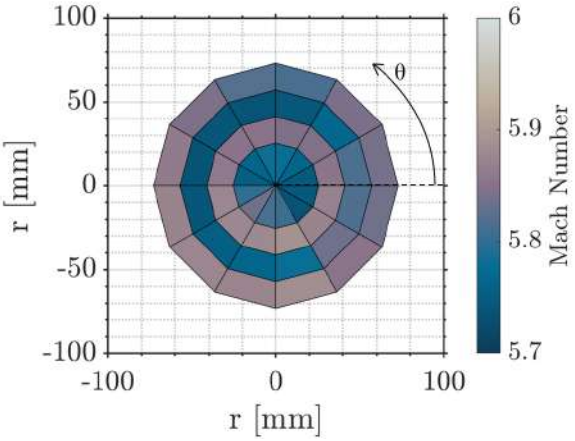

Fig. 10 Mach number contour at x = 1.30 m

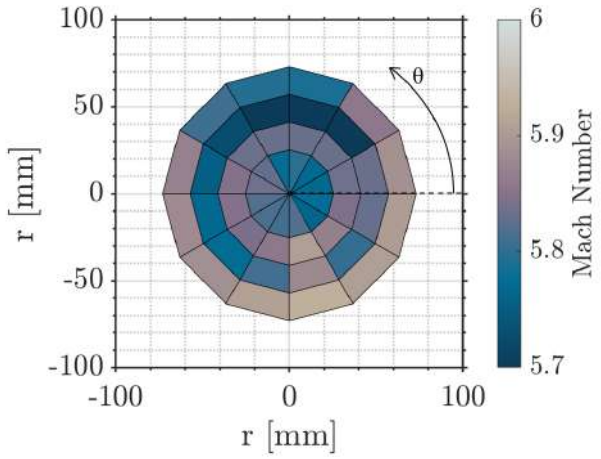

Fig. 11 Mach number contour at x = 1.15 m

Figure 12 compares the CFD simulation and the experimental measurements by overlaying the rake data from the 0° and 180° rays on top of the simulation results at the same axial locations. Overall, the pitot rake measurements show good agreement with the simulations and good Mach number uniformity.

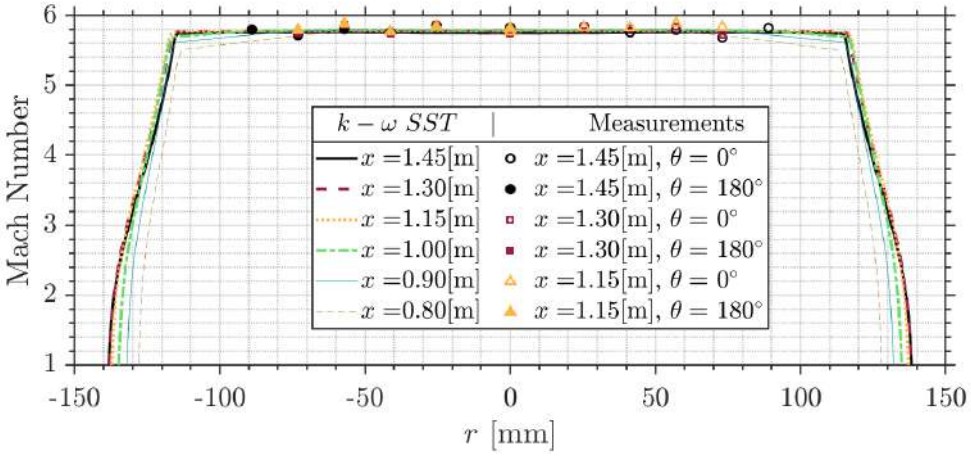

Fig. 12 Comparison between simulation and rake measurements

B. Noise Level Characterization

Freestream acoustic pressure fluctuations can heavily influence experimental results in hypersonic wind tunnels, primarily with regards to turbulent transition location on a research article [11]. Documenting pressure fluctuations in a hypersonic facility is therefore imperative information for future research performed in the facility. The ensemble averaged PSD's of the pressure fluctuations are shown in Fig. 13 at the center of the nozzle exit plane. The shaded portion around each PSD represents ±1 standard deviation from the mean PSD for a sample size of ten runs per condition.

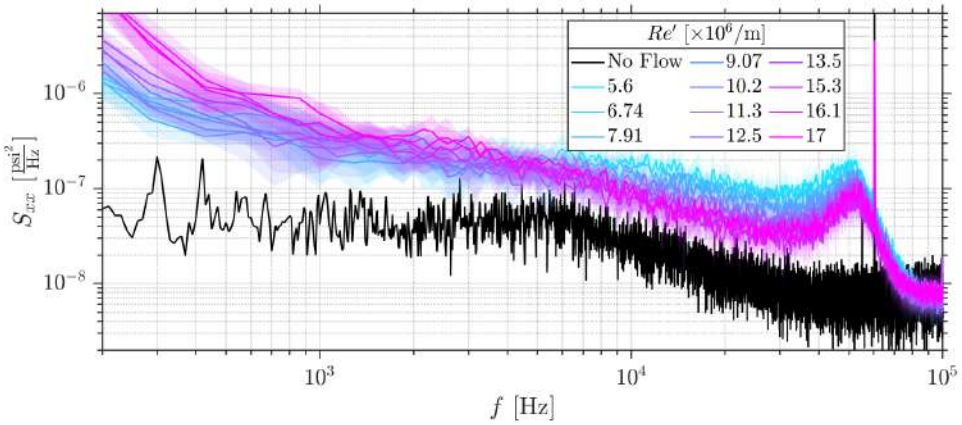

Fig. 13 PSD of pressure fluctuations at varying Re′ [$\times 10^6$ / m]

Noise levels were then computed via the method previously described for a sweep of freestream unit Reynolds numbers at each stagnation temperature, and are shown in Fig. 14.

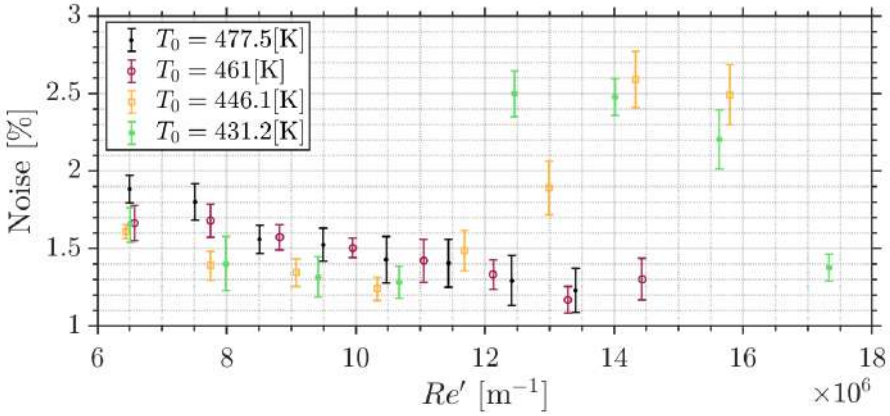

Fig. 14 Noise levels vs Re'

It is clear that freestream noise decreases with increasing unit Reynolds number for the stagnation temperature of 477.5K. This trend is likely a result of a fully turbulent nozzle wall boundary layer across all unit Reynolds numbers, while the mean normalization pressure continues to increase with increasing unit Reynolds number. This effect is directly observed in Fig. 15, where the fluctuation magnitudes appear to remain constant with respect to unit Reynolds number. The highest three unit Reynolds numbers in Fig. 15 were performed at a colder stagnation temperature and likely exhibit higher fluctuation variance due to liquefaction in the core flow.

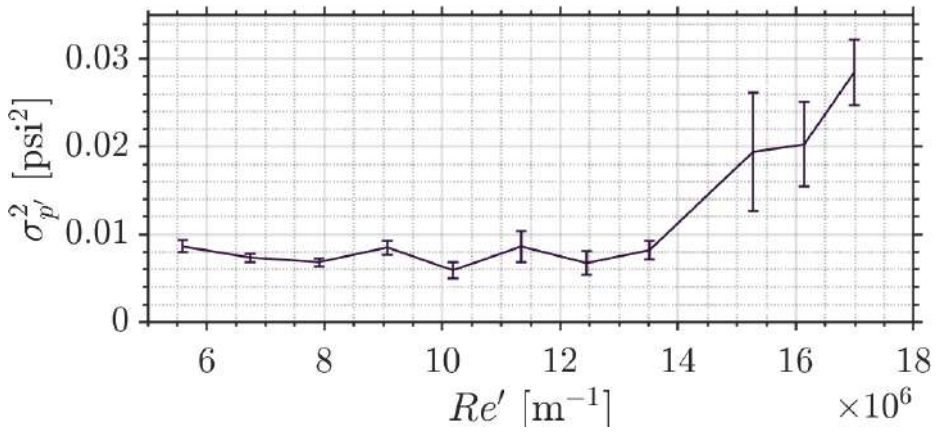

Fig. 15 Variance of pressure fluctuations, prior to normalization by mean pressure, for T_0 = 477.5 [K] (lowest 8 Re′) and for T_0 = 431.2 [K] (highest 3 Re′)

At the two coldest temperatures, the noise levels in Fig. 14 break the downward trend and begin to increase at the same freestream unit Reynolds numbers that the Mach number trends were observed to be broken in Fig. 7. This break of trend is again indicative of liquefaction and motivates future work in documenting the Notre Dame STEM Mach 6 Ludwieg Tube's operating envelope in terms of the stagnation conditions which begin to produce liquefaction. In order to achieve unit Reynolds numbers larger than $Re' = 14 \times 10^6$ m^{-1}, it was necessary to reduce the stagnation temperature due to structural limitations of the driver tube.

From the pitot rake measurements, for most instances, the noise could not be calculated due to the blockage of the rake. This blockage caused the tunnel to unstart before the standard deviation could completely converge. However, this was not the case for every run, and noise was calculated in the same manner as the single point probe. Figure 16 shows the calculated noise levels at the x = 1.30 m location across the ray $\theta = 0, 180$. From this figure, it is observed that the noise levels are consistent regardless of distance from the center of the nozzle. Other positions where noise was able to be calculated showed similar results with the noise levels being between ~1-2%, which is consistent and similar to the single point probe measurements at the same unit Reynolds' number, but is still on the relatively low end of noise levels.

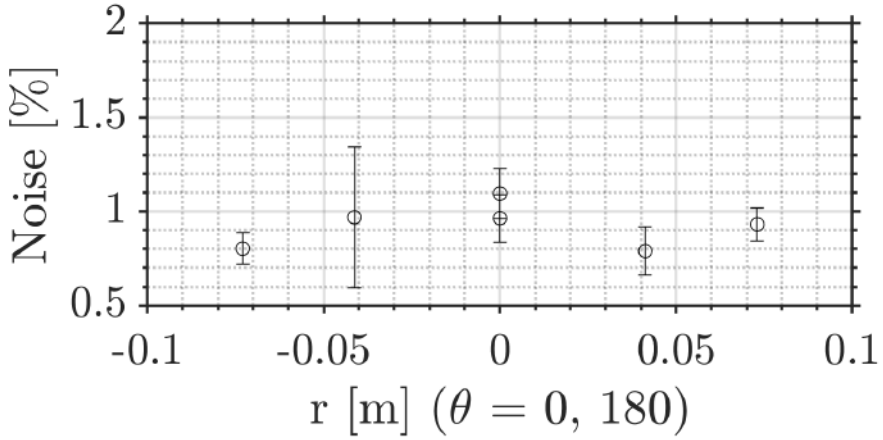

Fig. 16 Noise levels at x = 1.3 m and $\theta = 0°, 180°$

VI. Conclusion

A new facility was designed for the purpose of hypersonic research and education at The University of Notre Dame. The Notre Dame STEM Mach 6 Ludwieg Tube utilizes a plunger valve, that was designed in house, to actuate the tunnel. Once constructed, the tunnel was characterized using pitot pressures to find the Mach number and total pressure fluctuations of the flow. Results indicate good agreement with simulations, with a nominal Mach number of 5.8 across the core portion of the flow. Total pressure fluctuations were also computed, nominally at 1.5%, and were relatively constant across the flow. Additionally, the Mach and noise measurements were documented at varying Reynolds numbers. Through this relation, possible liquefaction of the air was found at low total temperatures and high Reynolds numbers.

Acknowledgments

The work was funded through a Department of Navy Award N00014-21-1-2522 on "Improving STEM Pathways through Realistic Scenarios, Analysis & Design and Hands-On Experience: A Pilot Curriculum for Hypersonic Systems" that was monitored by Dr. Michael Simpson.

References

[1] Estorf, M., Wolf, T., and Radespiel, R., "Experimental and Numerical Investigations on the Operation of the Hypersonic Ludwieg Tube Braunschweig," *Fifth European Symposium on Aerothermodynamics for Space Vehicles*, ESA Special Publication, Vol. 563, edited by D. Danesy, 2005, p. 579.

[2] Cable, A. J., and Cox, R. N., "The Ludwieg Pressure-Tube Supersonic Wind Tunnel," *Aeronautical Quarterly*, Vol. 14, No. 2, 1963, p. 143–157. https://doi.org/10.1017/S0001925900002729.

[3] Kimmel, R. L., Borg, M. P., Jewell, J. S., Lam, K.-Y., Bowersox, R. D., Srinivasan, R., Fuchs, S., and Mooney, T., *AFRL Ludwieg Tube Initial Performance*, 2017. https://doi.org/10.2514/6.2017-0102, URL https://arc.aiaa.org/doi/abs/10.2514/6.2017-0102.

[4] Hilton, W. F., "High Speed Wind Tunnel Testing. A. Pope and K. L. Goin. John Wiley 38;amp; Sons, London. 1965. 474 pp. Illustrations. 115s." *Journal of the Royal Aeronautical Society*, Vol. 70, No. 667, 1966, p. 739–739. https://doi.org/10.1017/S0001924000057213.

[5] Cummings, R., and McLaughlin, T., "Hypersonic Ludwieg tube design and future usage at the US Air Force Academy," *50th AIAA Aerospace Sciences Meeting including the New Horizons Forum and Aerospace Exposition*, 2012, p. 734.

[6] Sivells, J. C., "A computer program for the aerodynamic design of axisymmetric and planar nozzles for supersonic and hypersonic wind tunnels," Final Report, Dec. 1975 - Oct. 1977 ARO, Inc., Arnold Air Force Station, TN., Dec. 1978.

[7] Munoz, F., Wu, J., Radespiel, R., Semper, M., Cummings, R., Schilden, T., and Duan, L., *Freestream Disturbances Characterization in Ludwieg Tubes at Mach 6*, 2019. https://doi.org/10.2514/6.2019-0878.

[8] Steen, E. L., "Characterization and Development Of Nozzles For A Hypersonic Quiet Wind Tunnel," Master's thesis, Purdue University, 2010.

[9] Sweeney, C. J., "Characterization of a hypersonic quiet wind tunnel nozzle," Master's thesis, Purdue University, 2016.

[10] Ali, S. R. C., Zárate Cárdenas, R., Radespiel, R., Schilden, T., and Schröder, W., "Stagnation Point Probes in Hypersonic Flow," *New Results in Numerical and Experimental Fluid Mechanics XI*, 2017, pp. 117–127.

[11] Schneider, S. P., "Effects of High-Speed Tunnel Noise on Laminar-Turbulent Transition," *Journal of Spacecraft and Rockets*, 2001.